

TSPO-PET and diffusion-weighted MRI for imaging a mouse model of infiltrative human glioma

Hayet Pigeon, Elodie A. Pérès, Charles Truillet, Benoit Jego, Fawzi Boumezbeur, Fabien Caillé, Bastian Zinnhardt, Andreas H. Jacobs, Denis Le Bihan, and Alexandra Winkeler*

UMR 1023, IMIV, Service Hospitalier Frédéric Joliot, CEA, Inserm, Université Paris Sud, CNRS, Université Paris-Saclay, Orsay, France (H.P., C.T., B.J., F.C., A.W.); NeuroSpin, CEA/Université Paris-Saclay, Gif sur Yvette, France (E.A.P., F.B., D.L.B.); Normandie Université, UNICAEN, CEA, CNRS, ISTCT/CERVOxy Group, Caen, France (E.A.P.); EIMI and Department of Nuclear Medicine, University Hospital Münster, Westfälische Wilhelms University Münster, Münster, Germany (B.Z., A.H.J.); Department of Geriatrics, Johanniter Hospital, Evangelische Kliniken, Bonn, Germany (A.H.J.)

Corresponding Author: Alexandra Winkeler, PhD, CEA—Service Hospitalier Frédéric Joliot, 4, place du Général Leclerc, F-91401 ORSAY Cedex (alexandra.winkeler@cea.fr).

Abstract

Background. Glioblastoma (GBM) is the most devastating brain tumor. Despite the use of multimodal treatments, most patients relapse, often due to the highly invasive nature of gliomas. However, the detection of glioma infiltration remains challenging. The aim of this study was to assess advanced PET and MRI techniques for visualizing biological activity and infiltration of the tumor.

Methods. Using multimodality imaging, we investigated [¹⁸F]DPA-714, a radiotracer targeting the 18 kDa translocator protein (TSPO), [¹⁸F]FET PET, non-Gaussian diffusion MRI (apparent diffusion coefficient, kurtosis), and the S-index, a composite diffusion metric, to detect tumor infiltration in a human invasive glioma model. In vivo imaging findings were confirmed by autoradiography and immunofluorescence.

Results. Increased tumor-to-contralateral [¹⁸F]DPA-714 uptake ratios (1.49 ± 0.11) were found starting 7 weeks after glioma cell implantation. TSPO-PET allowed visualization of glioma infiltration into the contralateral hemisphere 2 weeks earlier compared with the clinically relevant biomarker for biological glioma activity [¹⁸F]FET. Diffusion-weighted imaging (DWI), in particular kurtosis, was more sensitive than standard T2-weighted MRI to detect differences between the glioma-bearing and the contralateral hemisphere at 5 weeks. Immunofluorescence data reflect in vivo findings. Interestingly, labeling for tumoral and stromal TSPO indicates a predominant expression of TSPO by tumor cells.

Conclusion. These results suggest that advanced PET and MRI methods, such as [¹⁸F]DPA-714 and DWI, may be superior to standard imaging methods to visualize glioma growth and infiltration at an early stage.

Key Points

1. Longitudinal TSPO-PET and diffusion MRI of a mouse model monitor infiltrative human glioma.
2. Early glioma detection with [¹⁸F]DPA-714 is compared with the clinical PET biomarker [¹⁸F]FET.

Glioblastoma (GBM) is the most common and aggressive form of primary human brain tumor. Although GBM therapy consists of aggressive multimodal treatments including surgery, radiation, and concomitant and adjuvant chemotherapy, the

currently available treatment options have limited efficacy.¹ Invasion of glioma cells into the surrounding brain parenchyma is a hallmark of GBM and one of the reasons for treatment failure.^{2,3} Imaging glioma cell infiltration remains challenging but

Importance of the Study

Invasiveness of glioma cells into the brain parenchyma is a major issue for failure of GBM treatment and tumor recurrence. However, common non-invasive imaging techniques fail to monitor these invading cells. Here, we report the use of TSPO-PET and DWI to follow tumor growth and invasion into the brain parenchyma using an invasively growing human GBM model. TSPO-PET

imaging accurately reflects GBM infiltration into the contralateral brain hemisphere, whereas diffusion kurtosis imaging detects early differences between the tumor and the contralateral brain parenchyma. This multimodality approach to monitor GBM invasiveness will improve the early detection of glioma invasion, help to assess therapy response, and be readily available for clinical translation.

advanced magnetic resonance imaging (MRI) and positron emission tomography (PET) might help in visualizing directly or indirectly the growth of diffuse GBMs.⁴

Diffusion-weighted imaging (DWI) probes tissue at a microscopic scale, well below image resolution, by measuring the interaction of diffusing water molecules with tissue elements. Hence, DWI reveals unique information about brain microarchitecture.⁵ By modeling the signal attenuation (S/S_0) using a non-Gaussian diffusion model,⁶ parametric maps can be computed for the apparent diffusion coefficient (ADC_0) and kurtosis. These non-Gaussian diffusion parameters can help distinguish malignant from benign lesions in a rat brain tumor model.⁷ Clinical studies have demonstrated that DWI parameters are helpful for grading gliomas by measuring the increased heterogeneity in more malignant tumors⁸ and could be relevant as predictive biomarkers of patients' outcome after treatment.^{9,10} Consistently, recent studies suggested the use of DWI to characterize tumor infiltration¹¹ and improve delineation of the tumor margin.¹² A novel composite diffusion metric, designed as a signature index (S-index) was proposed to distinguish tumoral from normal tissue. The S-index combines perfusion and diffusion parameters to enhance the sensitivity of DWI to assess tumor function and heterogeneity.¹³

Moreover, PET as a molecular imaging technique has been suggested as a promising alternative in glioma imaging, in particular for tumor growth and delineation of the tumor border.¹⁴ Recent preclinical imaging studies suggested PET imaging of the translocator protein of 18 kDa (TSPO) as a potential molecular imaging technique to improve tumor detection and possibly track glioma cell infiltration.^{15,16} Initial studies on TSPO and TSPO ligands in the brain indicated that the density of TSPO was high in malignant gliomas and glioma cell lines, but low in normal/unaffected brain tissue.^{17,18} Furthermore, TSPO expression levels positively correlated with the grade of malignancy and showed a negative correlation between TSPO expression and survival.^{19,20} Some results also propose TSPO as a marker of glioma invasiveness.^{21,22} TSPO expression can be monitored non-invasively using radiolabeled TSPO ligands. Several classes of TSPO radioligands have been developed in the last two decades, including the second generation TSPO tracer, N,N-diethyl-2-(2-(4-(2-[¹⁸F]fluoroethoxy)phenyl)-5,7-dimethylpyrazolo[1,5-a]pyrimidin-3-yl)acetamide ([¹⁸F]DPA-714). We and others have shown specific [¹⁸F]DPA-714 imaging in different models of rat glioma.²³⁻²⁵ Lately, a preclinical PET imaging study using another TSPO

radioligand, N-(2,5-dimethoxybenzyl)-2-[¹⁸F]-fluoro-N-(2-phenoxyphenyl)acetamide ([¹⁸F]PBR06), demonstrated elevated tracer uptake in human glioma xenotransplants according to the tumor grade and indicated infiltrative glioma growth not visible on conventional MRI.²⁶

We investigated the potential of TSPO-PET and diffusion-weighted MRI to assess glioma cell infiltration. Infiltrative glioma growth was monitored longitudinally alone and in combination with conventional T_2 -weighted imaging (T_2w) and DWI in a human invasively growing glioma model. We hypothesized that [¹⁸F]DPA-714 PET and DWI, in particular the composite S-index, can be used to (i) track glioma infiltration into the surrounding brain parenchyma and (ii) monitor glioma growth earlier than with T_2w MRI or the clinically established PET marker for endothelial amino acid transport, O-(2-¹⁸F-fluoroethyl)-L-tyrosine ([¹⁸F]FET).²⁷

Materials and Methods

Study Design and Animal Model

Longitudinal PET and combined PET/MRI studies were conducted to investigate the sensitivity and specificity of TSPO-PET as well as DWI to image infiltrative glioma growth. Animal studies were approved by the animal ethics committee of local authorities and were conducted in accordance with the ARRIVE (Animal Research: Reporting of In Vivo Experiments) guidelines and directives of the European Union on animal ethics and welfare. Male Naval Medical Research Institute nu/nu mice (Janvier Labs) 5–7 weeks old were housed in standard conditions under a regular 12-hour dark/light cycle. Food and water were available ad libitum. Stereotactically implanted were 2×10^5 human GBM cells in 1 μ L Neurobasal medium into the right striatum (2.5 mm lateral to the bregma and 3 mm deep) of the mice. In total, 27 mice were orthotopically implanted with human P3 cells and imaged at weeks 1, 3, 5, 7, and 9 post cell implantation (p.i.), respectively. A more detailed description is given in [Supplementary Figure 1](#). At the end of the last PET scan, mice were euthanized and brains were removed and frozen immediately for histology and autoradiography.

Cell Culture

The P3 human GBM cells used in the present study, obtained from Professor Hrvoje Miletic (Department of

Biomedicine, Translational Cancer Research, University of Bergen, Norway), were derived from one GBM patient (P3) and have previously been characterized in a human GBM-derived xenograft model in nude rats.²⁸ Glioma cells displayed typical growth patterns and phenotypes in vitro and in vivo. The cells were not further genetically authenticated. Cells were grown in Neurobasal medium containing x1 GlutaMax, x1 B27 supplement, 20 ng/mL basic fibroblast growth factor and epidermal growth factor, x1 penicillin/streptomycin (all from Gibco, Life Technologies), and 32 U/mL heparin (Panpharma) at 37°C in a 5% CO₂/95% air atmosphere.

Radiochemistry

[¹⁸F]DPA-714 and [¹⁸F]FET were synthesized as previously described.^{29,30} [¹⁸F]DPA-714 was obtained in 28 ± 5%, [¹⁸F]FET in 44 ± 7% decay corrected radiochemical yield with radiochemical purity above 99% and molar activity of 158 ± 68 GBq/μmol and 150 ± 51 GBq/μmol, respectively.

PET Acquisitions

During all experimental procedures, mice were anesthetized with isoflurane (3.0% for induction, 1.5–2% for maintenance of anesthesia) in 100% O₂. PET images were acquired on a Siemens Inveon small animal PET or PET-CT scanner. Both scanners were used in parallel in order to ensure a high specific radioactivity at the time of injection. Static PET scans were acquired 30–60 minutes after a tail vein injection of 8.2 ± 3.6 MBq [¹⁸F]DPA-714 or 7.2 ± 0.6 MBq [¹⁸F]FET. For attenuation correction, a CT or a transmission scan using an external 68-germanium point source was performed. Images were reconstructed using Fourier rebinning and a 2D ordered subset expectation maximization algorithm (16 subsets and 4 iterations). Except for the first timepoint (5 wk p.i.), PET image acquisition was performed within 24 h after MRI acquisition.

MRI Acquisitions

MRI experiments were conducted on an 11.7T Biospec MR scanner equipped with a CryoProbe dedicated for mouse brain imaging (Bruker BioSpin) as previously described.³¹ For more details see the Supplementary material.

Data Analysis

PET image analysis was performed using VINCI (v4.63.0; <http://www.nf.mpg.de/vinci3/>), a graphical image analysis package equipped with image co-registration tools.³² For quantitative analysis, a volume of interest (VOI) analysis was performed on the summed image datasets (30–60 min). Three VOIs were manually delineated, one around the tumor injection site in the ipsilateral hemisphere (T), one in the contralateral striatum (C), and one on the corpus callosum (CC). Ipsi- to contralateral and ipsilateral to CC ratios as well as standardized uptake values (SUVs) were calculated. The SUV is defined as tissue radioactivity

concentration in kBq/mL / ((injected dose in kBq) / (body-weight in g)).

For image co-registration [¹⁸F]DPA-714 PET-CT images were manually co-registered to the corresponding T₂w MRI and [¹⁸F]FET PET-CT images, respectively, using the contour and image co-registration tool of VINCI. A thresholding approach was applied on [¹⁸F]DPA-714 PET images as previously described,¹⁶ and detailed in the Supplementary material.

DWI data were processed using a homemade software implemented with MatLab (Mathworks) as previously described.³¹ Details can be found in the Supplementary material. For each animal, a region of interest (ROI) corresponding to the brain tumor (ipsilateral ROI) was manually delimited in the striatum on 3 consecutive slices, identified from the presence of the tumor cell injection site. For this ipsilateral ROI, the cell injection site identified by T2-hypointensity was excluded to avoid biasing the results. In the striatum of the hemisphere opposite to the tumor injection site, a contralateral ROI was delimited on the same slices. Mean values for ADC₀, kurtosis, and S-index for each ROI were calculated.

Autoradiography, Histology, and Immunohistochemistry

Frozen brain sections (20-μm thick) of whole tumor specimen were cut using a cryostat (Leica). Immunohistochemistry, autoradiography, and hematoxylin/eosin (H&E) staining were performed on adjacent 20-μm-thick brain sections as previously described³³ or according to the manufacturer's instructions (Labonord). For more details, see the Supplementary material.

Statistical Analysis

All data are presented as mean ± standard deviation. The statistical analyses were performed using GraphPad Prism software, v6.05. Comparisons of PET and DWI data between ipsilateral and contralateral VOIs over time were performed using a one-way ANOVA and Bonferroni multiple comparison tests for post hoc analysis. Differences in radiotracer uptake ratios ([¹⁸F]DPA-714, [¹⁸F]FET) were tested using a *t*-test. Significance levels were set at *P* < 0.05.

Results

Longitudinal [¹⁸F]DPA-714 PET Images of Human Invasive Glioma

PET imaging using the TSPO radioligand [¹⁸F]DPA-714 shows an increase in [¹⁸F]DPA-714 uptake in the ipsilateral (tumor-bearing) brain hemisphere over time. From 7 weeks p.i. onward, extended [¹⁸F]DPA-714 uptake in the ipsilateral hemisphere was observed. [¹⁸F]DPA-714 highlights infiltration of the tumor into the contralateral hemisphere via the CC after 7–9 weeks of glioma growth (Figure 1A, C). The mean SUVs after one (0.22 ± 0.06 vs 0.18 ± 0.04; *n* = 10), three (0.19 ± 0.06 vs 0.17 ± 0.06; *n* = 9), or five

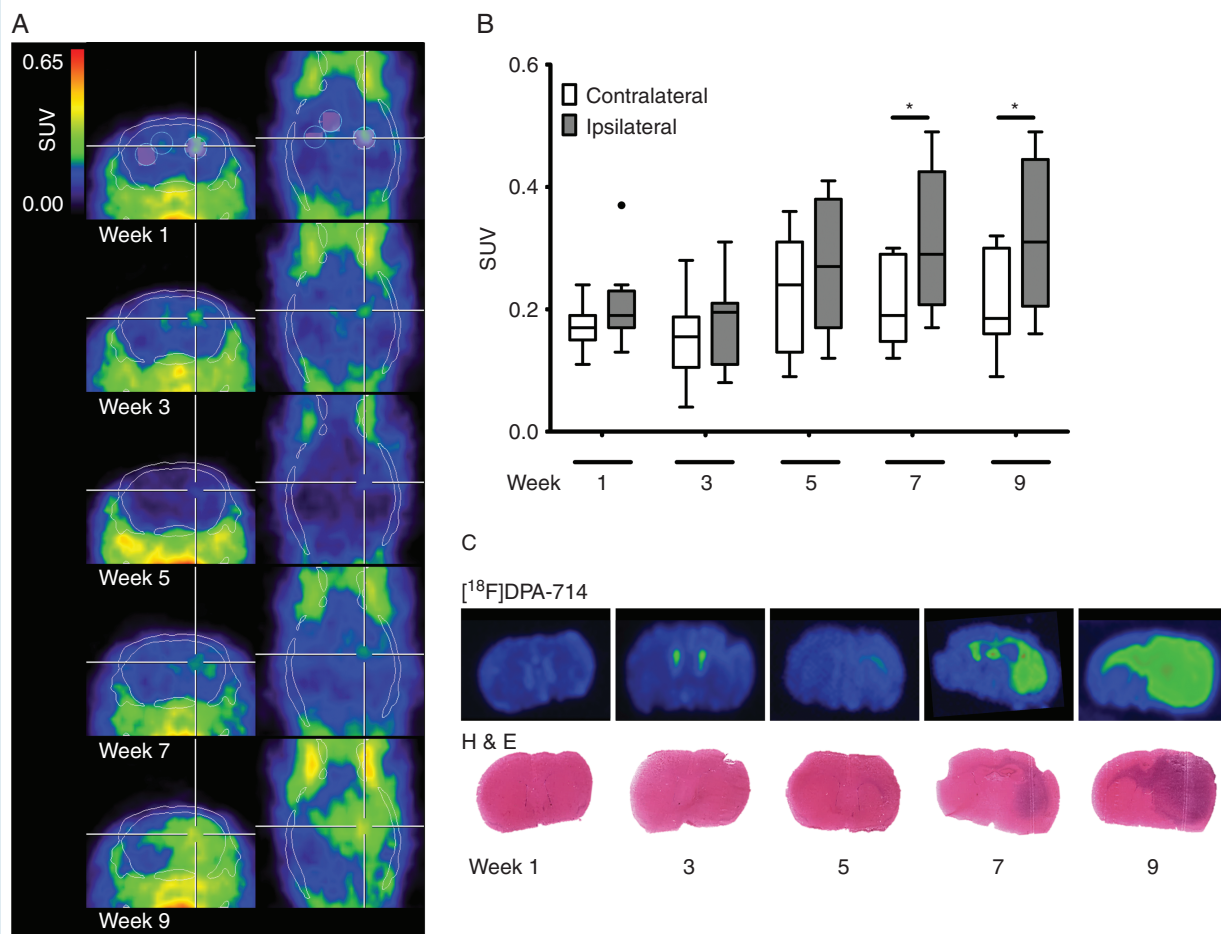


Fig. 1 Longitudinal TSPO-PET imaging, quantification, autoradiography, and histology of the human invasively growing P3 glioma model. (A) Summed [¹⁸F]DPA-714 PET images (30–60 min post injection) at 1, 3, 5, 7, and 9 weeks p.i. within the same animal indicated glioma growth and infiltration into the contralateral brain hemisphere. White lines represent CT skull contours, white and black circles ipsilateral, contralateral, and corpus callosum VOIs, respectively. (B) Tukey boxplot of ipsilateral and contralateral SUVs at the different imaging points displays significant differences between ipsi- and contralateral VOIs at 7 and 9 weeks p.i., respectively (**P* < 0.05; *n* = 10; • outlier). (C) Autoradiography and H&E staining of corresponding coronal mouse brain sections showing [¹⁸F]DPA-714 binding and tumor growth over time.

weeks (0.28 ± 0.11 vs 0.23 ± 0.10 ; *n* = 10) were not significantly different between ipsilateral and contralateral hemispheres, respectively. However, a significant increase in [¹⁸F]DPA-714 uptake is observed in the tumor-bearing hemisphere compared with the contralateral site at seven (SUV 0.31 ± 0.11 vs 0.21 ± 0.07 ; **P* < 0.05; *n* = 10) and nine weeks (0.32 ± 0.12 vs 0.21 ± 0.08 ; **P* < 0.05; *n* = 10) (Figure 1B). Ipsi-to-contralateral ratios rise over time showing significantly increased ratios at 7 and 9 weeks (Supplementary Figure 2A). In contrast, ipsilateral-to-CC ratios do not increase significantly but demonstrate significantly decreased values compared with ipsi- to contralateral at 9 weeks, indicating increased tracer uptake by invasive cells at the CC. Based on the applied thresholding, [¹⁸F]DPA-714 volumes significantly increased over time, reaching parts of the contralateral hemisphere (*****P* < 0.0001; *n* = 10; Supplementary Figure 2B). Validation of the in vivo imaging findings on brain sections using in vitro autoradiography with [¹⁸F]DPA-714 and H&E staining confirms glioma growth over

time, with infiltration of the tumor into the contralateral hemisphere, especially along the CC (Figure 1C).

Human TSPO as the Main Source of TSPO Expression in P3 Infiltrative Glioma

In vivo [¹⁸F]DPA-714 PET indicates tumor growth with infiltration into the contralateral brain hemisphere and significant differences regarding [¹⁸F]DPA-714 uptake or volume over time and between the injected and contralateral hemisphere from 7 weeks on. To investigate tumor development and contribution of different tumor components over time, immunohistochemistry was performed. Labeling of tumor cells with an anti-human Nestin antibody shows the presence of human glioma cells in the ipsilateral hemisphere and close to the CC as early as 3 weeks (Figure 2, hNestin). The labeling spreads within the ipsilateral site but also via the CC into the contralateral site at 5 weeks and extends in both brain hemispheres, but covers nearly the whole

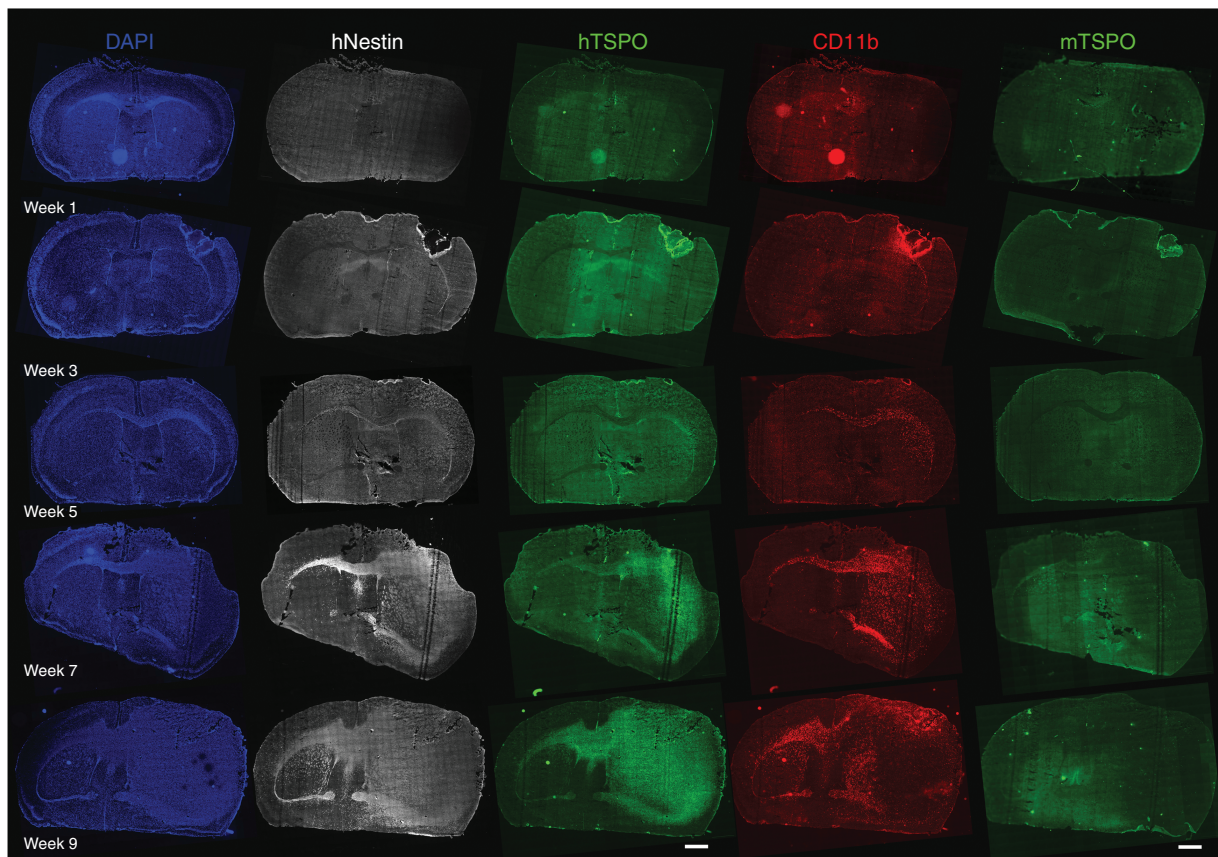


Fig. 2 Immunohistochemical distribution of human Nestin (hNestin), human TSPO (hTSPO), CD11b, and murine TSPO (mTSPO) in coronal slices of mouse brains at different timepoints after glioma cell injection. At 3 weeks p.i., hNestin and CD11b staining indicate the presence of human glioma cells and GAMS, respectively, in the ipsilateral brain hemisphere and in proximity to the CC. Human TSPO staining reveals the presence of hTSPO+ glioma cells from 5 weeks on (scale bar: 1000 μ m).

ipsilateral site at 7 and 9 weeks of glioma development. As [18 F]DPA-714 uptake reflects general TSPO expression, we employed 2 different antibodies, recognizing primarily the human or specifically the murine TSPO (hTSPO and mTSPO, respectively). Immunofluorescence images show faint hTSPO signal at 3 weeks, which, similar to the Nestin labeling, becomes clearly visible at 5 weeks in the ipsilateral hemisphere and its part of the CC (Figure 2, hTSPO). Comparable to Nestin and in line with the *in vivo* findings, the hTSPO staining propagates within the ipsilateral and via the CC into the contralateral hemisphere at 7 and 9 weeks. In contrast, mTSPO staining is barely visible on the overview scans (Figure 2, mTSPO). Higher resolution images indicate only limited signal within the tumor core or the infiltrative zone (Supplementary Figure 3). Labeling of glioma-associated microglia/macrophages (GAMS) as a possible source of mTSPO indicates the presence of CD11b+ GAMS as early as 3 weeks around the injection site as well as in the ipsilateral hemisphere and the corresponding CC (Figure 2, CD11b). The signal evolves from there into neighboring regions and into the contralateral hemisphere at 5, 7, and 9 weeks, underlining the abundance of CD11b+ GAMS in and around the tumor. Only individual CD11b+ cells are

also mTSPO+, whereas the majority lack TSPO expression (Supplementary Figure 3). Less CD11b+ GAMS are present within the tumor after week 9 (Figure 2, CD11b).

[18 F]DPA-714 Detects Invasively Growing Glioma Before the Clinically Established Radiotracer [18 F]FET

To compare [18 F]DPA-714 PET with the clinically established tracer for endothelial amino acid transport, [18 F]FET, PET images for [18 F]FET were acquired in addition to [18 F]DPA-714 at 7 and 9 weeks. As reported above, extended [18 F]DPA-714 signal is found in the ipsilateral hemisphere at 7 weeks. In contrast, no significant signal for [18 F]FET uptake can be demonstrated in the glioma-bearing compared with the contralateral hemisphere at this timepoint ($P = 0.76$; Figure 3). [18 F]FET SUVs were 0.36 ± 0.11 versus 0.36 ± 0.13 (ipsi- vs contralateral, respectively; $n = 5$), with an ipsi- to contralateral ratio of 1.04 ± 0.11 . Comparison of [18 F]DPA-714 and [18 F]FET uptake at 9 weeks shows an increased [18 F]FET uptake in the ipsilateral hemisphere with SUVs of 0.55 and 0.96 compared with SUVs of 0.45 and 0.64, respectively, at the contralateral side ($n = 2$). In contrast to [18 F]DPA-714, [18 F]FET

uptake at 9 weeks is found in a restricted area in the ipsilateral but not in the contralateral site (Figure 3, week 9).

TSPO-PET and Diffusion MRI Allow Early Detection of Invasively Growing Glioma

The results of the longitudinal [^{18}F]DPA-714 PET study demonstrate a significant change in [^{18}F]DPA-714 uptake from 7

weeks after tumor implantation. Based on these results, a second study combining [^{18}F]DPA-714 PET with anatomic T_2 w- and diffusion MRI was performed in order to investigate particularly glioma growth between 5 and 9 weeks. [^{18}F]DPA-714 uptake at 5 weeks shows faint PET signal localized around the injection tract (Figure 4A) with SUVs of 0.20 ± 0.02 and 0.17 ± 0.02 for ipsi- and contralateral VOIs, respectively ($n = 7$). Similar to the first longitudinal study, a significant increase in [^{18}F]DPA-714 uptake in the

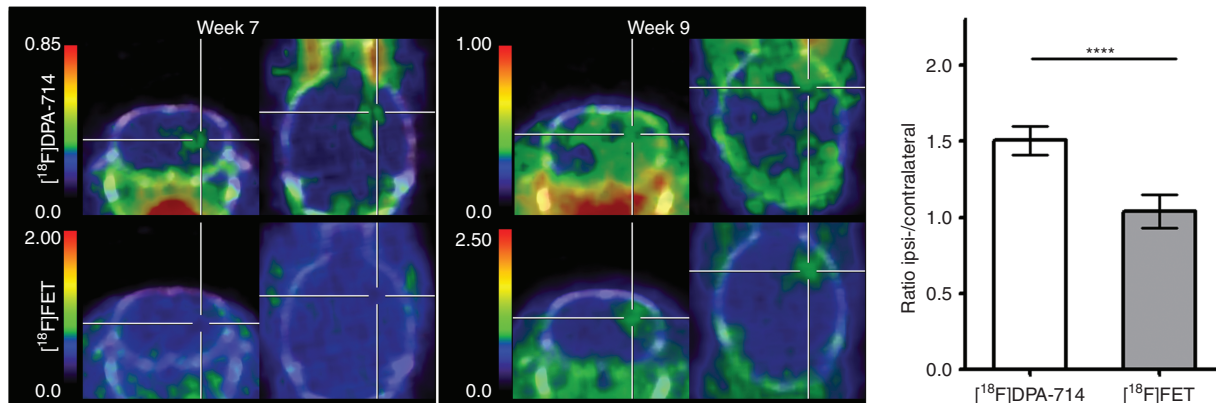


Fig. 3 Comparison of [^{18}F]DPA-714 and [^{18}F]FET imaging of the human invasively growing P3 glioma model. PET images were performed at 7 and 9 weeks p.i. Summed [^{18}F]DPA-714 and [^{18}F]FET PET images (30–60 min p.i.) of the same tumor-bearing animals demonstrate early tumor detection at 7 weeks using [^{18}F]DPA-714 but not [^{18}F]FET. [^{18}F]FET uptake was only detected in a restricted area at 9 weeks p.i. Ipsi- to contralateral uptake ratios were significantly higher for [^{18}F]DPA-714 compared with [^{18}F]FET (**** $P < 0.0001$).

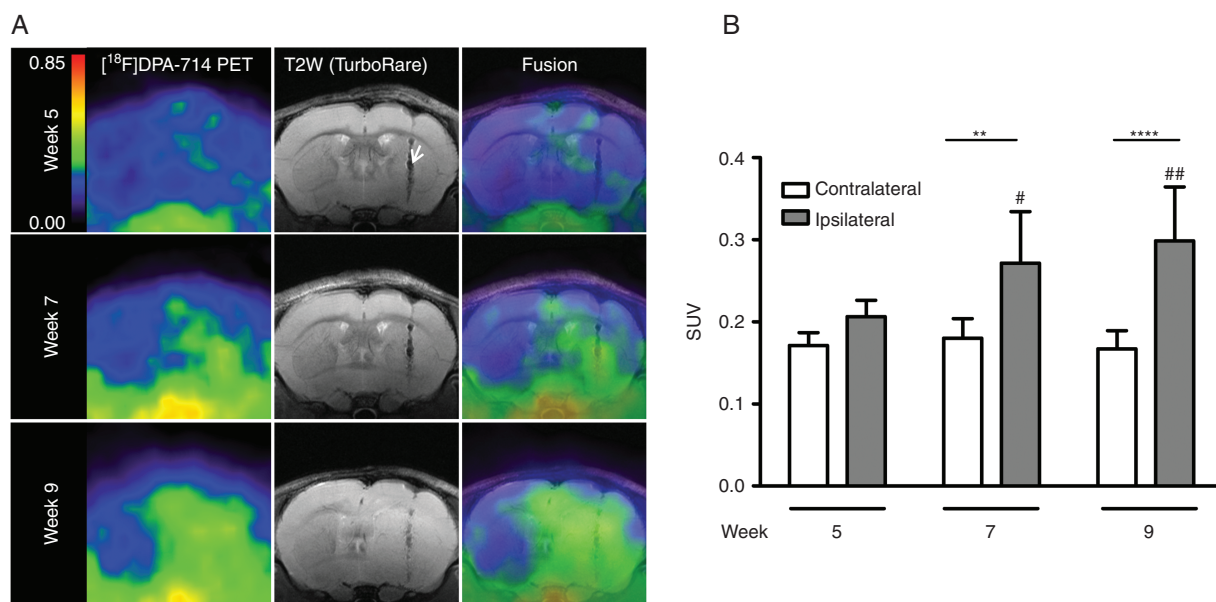


Fig. 4 Co-registration of TSPO-PET signal with anatomic T_2 w MRI. (A) (Left) Summed [^{18}F]DPA-714 PET images (30–60 min p.i.) at 5, 7, and 9 weeks of tumor development. (Middle) Anatomic T_2 w images. The white arrow indicates the needle tract from tumor cell implantation. (Right) Fused [^{18}F]DPA-714 PET/ T_2 w MRI images. (B) Quantification of SUVs of ipsilateral and contralateral VOIs at the different imaging points. [^{18}F]DPA-714 uptake increase in the ipsilateral compared with the contralateral hemisphere is observed at 7 and 9 weeks p.i. (**week 7: $P < 0.01$; $n = 7$ and ****week 9: $P < 0.0001$; $n = 7$) and even in the ipsilateral hemisphere over time (##week 9 vs 5: $P < 0.01$ and #week 7 vs 5: $P < 0.05$).

ipsilateral hemisphere is observed at 7 and 9 weeks (Figure 4B) with SUVs of 0.27 ± 0.06 versus 0.18 ± 0.02 (week 7: ipsi- vs contralateral, respectively; $**P < 0.01$; $n = 7$) and 0.30 ± 0.07 versus 0.17 ± 0.02 (week 9: $****P < 0.0001$; $n = 7$). As observed before, 9 weeks p.i. the [^{18}F]DPA-714 PET signal indicates a massive tumor involving nearly the complete ipsilateral brain hemisphere, including infiltration into the contralateral side. SUVs in the tumor-implanted site were significantly increased at 9 ($##P < 0.01$) and 7 ($\#P < 0.05$) weeks compared with week 5. The corresponding T_2w anatomic MR images depict the needle tract from tumor cell implantation (Figure 4A, white arrow), whereas hyperintense areas corresponding to tumor edema can only be seen 9 weeks p.i. Precise boundaries of the tumor are especially difficult to define.

Non-Gaussian diffusion parameters such as the ADC_0 and kurtosis, as well as the composite marker S-index, provide information on a different level that is tissue microstructure, while information provided by PET is more functional in nature. Whereas parametric maps of the ADC_0 do not show any significant change in the tumor-bearing hemisphere or elsewhere in the brain, kurtosis and S-index parametric maps indicate increased values in the ipsilateral hemisphere and at the site of the CC (Figure 5A). Comparison of ipsilateral versus contralateral ADC_0 , kurtosis, or S-index values demonstrates significantly increased values for ipsilateral kurtosis and S-index, whereas no significant differences have been

seen for ADC_0 (Figure 5B). Ipsilateral kurtosis values are significantly higher compared with the contralateral site from 5 weeks p.i. (0.79 ± 0.02 vs 0.74 ± 0.02 ; $***P < 0.001$, 0.82 ± 0.01 vs 0.76 ± 0.02 ; $***P < 0.001$, 0.88 ± 0.03 vs 0.76 ± 0.02 ; $****P < 0.0001$, at 5, 7, and 9 weeks p.i., respectively). Likewise, the S-index shows a significant ipsilateral increase compared with the contralateral side at week 9 (48.30 ± 5.30 vs 32.35 ± 4.31 ; $**P < 0.01$); however, no difference between the tumor-implanted and the contralateral side is found at week 5 (34.82 ± 8.24 vs 32.02 ± 7.91) or week 7 (40.43 ± 3.97 vs 34.12 ± 3.65). Furthermore, ipsilateral kurtosis and S-index are augmented at 9 compared with 5 ($****P < 0.0001$ and $##P < 0.01$) and 7 weeks ($$$P < 0.01$, kurtosis only), respectively (Figure 5B).

Discussion

In this study we investigated the feasibility of [^{18}F]DPA-714 PET in combination with diffusion MRI to follow glioma growth and cell infiltration over time in a human invasively growing glioma model. We could demonstrate that longitudinal TSPO-PET imaging allows monitoring and accurate reflection of glioma growth and infiltration. Moreover, DWI and [^{18}F]DPA-714 PET were superior over conventional T_2w MRI or [^{18}F]FET PET in early detection of the tumor

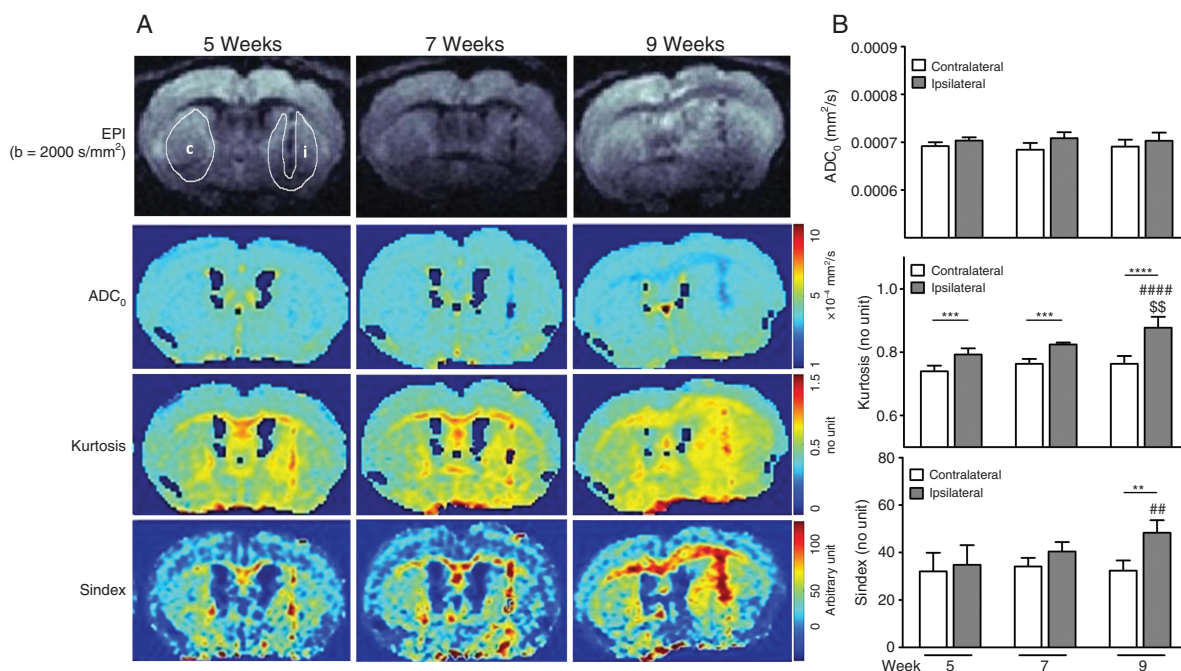


Fig. 5 Longitudinal DWI in brain of mice bearing infiltrative glioma. (A) ADC_0 , kurtosis, and S-index mapping determined by a non-Gaussian diffusion model on echo-planar imaging at different points. (B) Comparison of ipsilateral versus contralateral ADC_0 , kurtosis, or S-index values at 5, 7, and 9 weeks. Significantly increased ipsilateral kurtosis (5, 7, and 9 wk) and S-index (9 wk) are observed compared with contralateral values ($**P < 0.01$, $***P < 0.001$, and $****P < 0.0001$), whereas no significant differences were observed for ADC_0 . Considering the ipsilateral region only, S-index and kurtosis are also significantly higher at 9 compared with 5 ($##P < 0.01$ and $****P < 0.0001$) and 7 weeks of tumor growth ($$$P < 0.01$, kurtosis only).

and tumor infiltration, respectively. Autoradiography and immunohistochemistry confirmed the presence of an invasively growing tumor as well as distinct TSPO expression closely reflecting tumor growth and infiltration. Tumor growth will yield in changes of cellular density (to which diffusion MRI is sensitive) and vascularization, thus increasing TSPO receptor density and perfusion. However, previous *in vivo* displacement studies in glioma models demonstrated TSPO specificity.^{25,34}

It is well known that high-grade gliomas extensively infiltrate into the brain parenchyma. However, glioma cell infiltration is usually not detectable by conventional clinical MRI (T_2w , T_1w MRI, with or without gadolinium).² Recently, several groups suggested the potential of TSPO-PET for glioma imaging.^{15,25,34} PET or SPECT imaging targeting the translocator protein is a well-known technique for imaging of neuroinflammation as activated microglia highly express TSPO. The fact that some of the recently developed so-called second generation TSPO radioligands have already been translated and assessed in clinical studies of neurodegenerative diseases^{35–37} would therefore facilitate application of TSPO imaging in human gliomas.

TSPO expression in the glioma-bearing brain can be of different origins. Specifically in the orthotopic animal model, due to the surgical intervention, inflammatory TSPO may contribute, although sham-operated animals did not show significant tracer uptake.^{16,25} We and others have lately shown that the main source of TSPO expression in gliomas is related to neoplastic cells.^{15,25} However, also GAMs contribute to the TSPO signal.^{16,23} Although individual TSPO+ GAMs could be detected within and around the tumor, we show predominant TSPO expression by tumor cells in this human invasive glioma model. Interestingly, we also found an abundant number of TSPO-GAMs specifically at the tumor border.

Depending on the literature, 60–85% of glioma patients express TSPO at moderate to high level^{19,20,26} and TSPO imaging would be of value for those patients. Even though kurtosis and the composite S-index did not monitor glioma infiltration as early as [¹⁸F]DPA-714 PET, imaging of infiltration into the contralateral hemisphere is improved compared with T_2w MRI. Furthermore, kurtosis and even the composite S-index may be well suited for early tumor detection and to some extent infiltration (although to a later timepoint) in patients with TSPO-negative GBM or in medical centers without access to PET scanners.

Recent studies suggest that diffusion kurtosis imaging may be useful for differentiating glioma grades and detecting microstructural changes in gliomas.^{38,39} Kurtosis reflects the heterogeneous diffusion environments experienced by water molecules as they encounter barriers, move between compartments, and undergo chemical exchange. Thus, this parameter could be sensitive to microstructural modifications of the cerebral parenchyma induced by invasive tumor cells. However, no studies have been evaluated whether kurtosis detects areas of glioma invasion. In this invasive glioma model, we show for the first time that kurtosis is very sensitive for tumor detection, as indicated by its early increase in the tumor-bearing

hemisphere. We also demonstrate that the S-index, a new metric diffusion combining all DWI parameters, is promising in detection of invasive glioma. In contrast to current approaches based on fitting of DWI signals, which require iterative calculations using complex equations, the quantification of the S-index based on only 2 key b-values is direct and easy, making the processing time extremely short and compatible with real-time processing in clinical practice.

The other important finding within this study is the advanced/early detection of the invasively growing glioma using [¹⁸F]DPA-714 PET and DWI in comparison to conventional T_2w MRI or the clinical imaging biomarker for assessing glioma extent, [¹⁸F]FET. This result is in accordance with the findings by Jensen and colleagues on TSPO-SPECT imaging in 3 GBM patients, who observed tumor expansion predominantly in areas of high [¹²³I]CLINDE binding compared with [¹⁸F]FET PET and contrast-enhanced structural MRI.⁴⁰ Also the multitracer imaging approach from Zinnhardt et al that compared [¹⁸F]DPA-714, [¹⁸F]BR-351, and [¹⁸F]FET in a murine model of glioma indicated a unique area of [¹⁸F]DPA-714 positive glioma tissue, with no [¹⁸F]FET uptake.¹⁶ Taking into account the clinical TSPO-SPECT data⁴⁰ and results from a preclinical TSPO-PET study using human glioma xenotransplants,²⁶ the authors suggested that the unique tissue areas at the tumor margins are of high interest, as they might be related to sites of glioma infiltration, an aspect supported by the outcome of the present study.

Quantification of TSPO-PET bears some challenges, such as the different binding affinity patterns for the second generation TSPO ligands in humans due to a genetic polymorphism in the *tspo* gene,⁴¹ the question of a suitable reference region for quantification of TSPO binding, and the impact of the vascular component for TSPO quantification.⁴² However, results from the present study as well as the recent preclinical and clinical findings should encourage further investigation of TSPO-PET for glioma imaging, in particular for tumor infiltration, as limitations may be tackled, such as by accounting for the vascular compartment⁴³ and including genotyping of patients for clinical TSPO-PET studies.

In conclusion, this study strongly supports the high promise of clinical translation of [¹⁸F]DPA-714 PET to improve delineation of infiltrative components or glioma-associated inflammation as confirmed by kurtosis-based diffusion imaging, which seems to be complementary to other established molecular imaging markers for gliomas.

Supplementary Material

Supplementary data are available at *Neuro-Oncology* online.

Keywords

[¹⁸F]DPA-714 | glioma | diffusion MRI | S-index | TSPO

Funding

This work was supported by Agence National de la Recherche (ANR-11-INBS-0006) and EU Seventh Framework Programme (FP7/2007–2013, HEALTH-F2-2011–278850 [INMiND]).

Acknowledgments

The authors thank Emilie Jaumain and Stephane Demphel for their excellent technical support as well as Raphael Boisgard for scientific discussions during the project. We are grateful to Dr Makoto Higuchi for kindly providing the rodent specific anti-TSPO antibody NP155 and Dr Hrvoje Miletic for the P3 cells.

Conflict of interest statement. None declared.

Authorship statement: Conception and design: HP, EAP, AW. Methodology development: HP, BJ, DLB, AW. Data acquisition: HP, EAP, BJ, CT, FC, AW. Data analysis/interpretation: HP, EAP, CT, FB, BZ, AHJ, DLB, AW. Manuscript writing, review, revision: HP, EAP, CT, FB, FC, BZ, AHJ, AW. Radiotracer production and quality: FC

References

- Omuro A, DeAngelis LM. Glioblastoma and other malignant gliomas: a clinical review. *JAMA*. 2013;310(17):1842–1850.
- Claes A, Idema AJ, Wesseling P. Diffuse glioma growth: a guerilla war. *Acta Neuropathol*. 2007;114(5):443–458.
- Dunn GP, Rinne ML, Wykosky J, et al. Emerging insights into the molecular and cellular basis of glioblastoma. *Genes Dev*. 2012;26(8):756–784.
- Dhermain FG, Hau P, Lanfermann H, Jacobs AH, van den Bent MJ. Advanced MRI and PET imaging for assessment of treatment response in patients with gliomas. *Lancet Neurol*. 2010;9(9):906–920.
- Le Bihan D, lima M. Diffusion magnetic resonance imaging: what water tells us about biological tissues. *PLoS Biol*. 2015;13(7):e1002203.
- lima M, Yano K, Kataoka M, et al. Quantitative non-Gaussian diffusion and intravoxel incoherent motion magnetic resonance imaging: differentiation of malignant and benign breast lesions. *Invest Radiol*. 2015;50(4):205–211.
- lima M, Reynaud O, Tsurugizawa T, et al. Characterization of glioma microcirculation and tissue features using intravoxel incoherent motion magnetic resonance imaging in a rat brain model. *Invest Radiol*. 2014;49(7):485–490.
- Maximov II, Tonoyan AS, Pronin IN. Differentiation of glioma malignancy grade using diffusion MRI. *Phys Med*. 2017;40:24–32.
- Galbán S, Lemasson B, Williams TM, et al. DW-MRI as a biomarker to compare therapeutic outcomes in radiotherapy regimens incorporating temozolomide or gemcitabine in glioblastoma. *PLoS One*. 2012;7(4):e35857.
- Schmainda KM. Diffusion-weighted MRI as a biomarker for treatment response in glioma. *CNS Oncol*. 2012;1(2):169–180.
- Price SJ, Jena R, Burnet NG, et al. Improved delineation of glioma margins and regions of infiltration with the use of diffusion tensor imaging: an image-guided biopsy study. *AJNR Am J Neuroradiol*. 2006;27(9):1969–1974.
- Lutz K, Wiestler B, Graf M, et al. Infiltrative patterns of glioblastoma: identification of tumor progress using apparent diffusion coefficient histograms. *J Magn Reson Imaging*. 2014;39(5):1096–1103.
- lima M, Le Bihan D. Clinical intravoxel incoherent motion and diffusion mr imaging: past, present, and future. *Radiology*. 2016;278(1):13–32.
- la Fougère C, Suchorska B, Bartenstein P, Kreth FW, Tonn JC. Molecular imaging of gliomas with PET: opportunities and limitations. *Neuro Oncol*. 2011;13(8):806–819.
- Roncaroli F, Su Z, Herholz K, Gerhard A, Turkheimer FE. TSPO expression in brain tumours: is TSPO a target for brain tumour imaging? *Clin Transl Imaging*. 2016;4:145–156.
- Zinnhardt B, Pigeon H, Theze B, et al. Combined PET imaging of the inflammatory tumor microenvironment identifies margins of unique radio-tracer uptake. *Cancer Res*. 2017;77:1831–1841.
- Black KL, Ikezaki K, Santori E, Becker DP, Vinters HV. Specific high-affinity binding of peripheral benzodiazepine receptor ligands to brain tumors in rat and man. *Cancer*. 1990;65(1):93–97.
- Cornu P, Benavides J, Scatton B, Hauw JJ, Philippon J. Increase in omega 3 (peripheral-type benzodiazepine) binding site densities in different types of human brain tumours. A quantitative autoradiography study. *Acta Neurochir (Wien)*. 1992;119(1–4):146–152.
- Miettinen H, Kononen J, Haapasalo H, et al. Expression of peripheral-type benzodiazepine receptor and diazepam binding inhibitor in human astrocytomas: relationship to cell proliferation. *Cancer Res*. 1995;55(12):2691–2695.
- Vlodavsky E, Soustiel JF. Immunohistochemical expression of peripheral benzodiazepine receptors in human astrocytomas and its correlation with grade of malignancy, proliferation, apoptosis and survival. *J Neurooncol*. 2007;81(1):1–7.
- Rechichi M, Salvetti A, Chelli B, et al. TSPO over-expression increases motility, transmigration and proliferation properties of C6 rat glioma cells. *Biochim Biophys Acta*. 2008;1782(2):118–125.
- Veenman L, Levin E, Weisinger G, et al. Peripheral-type benzodiazepine receptor density and in vitro tumorigenicity of glioma cell lines. *Biochem Pharmacol*. 2004;68(4):689–698.
- Awde AR, Boisgard R, Thézé B, et al. The translocator protein radioligand 18F-DPA-714 monitors antitumor effect of erufosine in a rat 9L intracranial glioma model. *J Nucl Med*. 2013;54(12):2125–2131.
- Tang D, Hight MR, McKinley ET, et al. Quantitative preclinical imaging of TSPO expression in glioma using N,N-diethyl-2-(4-(2-(18F-fluoroethoxy)phenyl)-5,7-dimethylpyrazolo[1,5-a]pyrimidin-3-yl)acetamide. *J Nucl Med*. 2012;53(2):287–294.
- Winkeler A, Boisgard R, Awde AR, et al. The translocator protein ligand [¹⁸F]DPA-714 images glioma and activated microglia in vivo. *Eur J Nucl Med Mol Imaging*. 2012;39(5):811–823.
- Buck JR, McKinley ET, Fu A, et al. Preclinical TSPO ligand PET to visualize human glioma xenotransplants: a preliminary study. *PLoS One*. 2015;10(10):e0141659.
- Langen KJ, Galldiks N, Hattingen E, Shah NJ. Advances in neuro-oncology imaging. *Nat Rev Neurol*. 2017;13(5):279–289.
- Keunen O, Johansson M, Oudin A, et al. Anti-VEGF treatment reduces blood supply and increases tumor cell invasion in glioblastoma. *Proc Natl Acad Sci U S A*. 2011;108(9):3749–3754.

29. Damont A, Hinnen F, Kuhnast B, et al. Radiosynthesis of [F-18] DPA-714, a selective radioligand for imaging the translocator protein (18 kDa) with PET. *J Labelled Comp Radiopharm.* 2008;51(7–8):286–292.
30. Bourdier T, Gregoric I, Roselt P, Jackson T, Faragalla J, Katsifis A. Fully automated one-pot radiosynthesis of O-(2-[18F]fluoroethyl)-L-tyrosine on the TracerLab FX(FN) module. *Nucl Med Biol.* 2011;38(5):645–651.
31. Peres EA, Etienne O, Grigis A, Boumezbeur F, Boussin FD, Le Bihan D. Longitudinal study of irradiation-induced brain microstructural alterations with S-index, a diffusion MRI biomarker, and MR spectroscopy. *Int J Radiat Oncol Biol Phys.* 2018;102:1244–1254.
32. Vollmar SCJ, Sue M, Klein J, Jacobs AH, Herholz K. *VINCI—Volume Imaging in Neurological Research, Co-Registration and ROIs Forschung und wissenschaftliches Rechnen 2003.* Göttingen, Germany: Gesellschaft für wissenschaftliche Datenverarbeitung; 2004:115–131.
33. Pottier G, Gómez-Vallejo V, Padro D, et al. PET imaging of cannabinoid type 2 receptors with [11C]A-836339 did not evidence changes following neuroinflammation in rats. *J Cereb Blood Flow Metab.* 2017;37(3):1163–1178.
34. Buck JR, McKinley ET, Hight MR, et al. Quantitative, preclinical PET of translocator protein expression in glioma using 18F-N-fluoroacetyl-N-(2,5-dimethoxybenzyl)-2-phenoxyaniline. *J Nucl Med.* 2011;52(1):107–114.
35. Hamelin L, Lagarde J, Dorothée G, et al; Clinical IMABio3 team. Early and protective microglial activation in Alzheimer's disease: a prospective study using 18F-DPA-714 PET imaging. *Brain.* 2016;139(Pt 4):1252–1264.
36. Kreisl WC, Lyoo CH, Liow JS, et al. (11)C-PBR28 binding to translocator protein increases with progression of Alzheimer's disease. *Neurobiol Aging.* 2016;44:53–61.
37. Dupont A-C, Largeau B, Santiago Ribeiro M, Guilloteau D, Tronel C, Arlicot N. Translocator protein-18 kDa (TSPO) positron emission tomography (PET) imaging and its clinical impact in neurodegenerative diseases. *Int J Mol Sci.* 2017;18(4):785.
38. Li F, Shi W, Wang D, et al. Evaluation of histopathological changes in the microstructure at the center and periphery of glioma tumors using diffusional kurtosis imaging. *Clin Neurol Neurosurg.* 2016;151:120–127.
39. Qi XX, Shi DF, Ren SX, et al. Histogram analysis of diffusion kurtosis imaging derived maps may distinguish between low and high grade gliomas before surgery. *Eur Radiol.* 2018;28(4):1748–1755.
40. Jensen P, Feng L, Law I, et al. TSPO imaging in glioblastoma multiforme: a direct comparison between 123I-CLINDE SPECT, 18F-FET PET, and gadolinium-enhanced MR imaging. *J Nucl Med.* 2015;56(9):1386–1390.
41. Owen DR, Yeo AJ, Gunn RN, et al. An 18-kDa translocator protein (TSPO) polymorphism explains differences in binding affinity of the PET radioligand PBR28. *J Cereb Blood Flow Metab.* 2012;32(1):1–5.
42. Rizzo G, Veronese M, Tonietto M, Zanotti-Fregonara P, Turkheimer FE, Bertoldo A. Kinetic modeling without accounting for the vascular component impairs the quantification of [(11)C]PBR28 brain PET data. *J Cereb Blood Flow Metab.* 2014;34(6):1060–1069.
43. Veronese M, Reis Marques T, Bloomfield PS, et al. Kinetic modelling of [(11)C]PBR28 for 18 kDa translocator protein PET data: a validation study of vascular modelling in the brain using XBD173 and tissue analysis. *J Cereb Blood Flow Metab.* 2017;38:1227–1242.